Modulation of Turbulent Boundary Layer by EHD Flows

Alfredo Soldati
Centro di Fluidodinamica e Idraulica
Università di Udine, 33100 Udine
ITALY

Abstract

Ionic species dispersed in a fluid under the action of an electric field drive electrohydrodynamic (EHD) flows. EHD flows in gases occur frequently in electrostatic precipitators (ESP), where dispersed ions are required to charge the initially neutral dust particles which are to be separated. EHD flows are believed to be detrimental for dust collection in ESPs. In this work, we look at EHD flows from a new perspective and we examine the possibility of tuning their intensity and geometry in order to modify turbulence structure. Specifically, we follow a recent idea (Schoppa and Hussain, 1998), in which idealized large-scale, streamwise vortical flows were applied to reduce turbulent drag in a boundary layer and we suggest a new configuration for ESPs which could be optimized for drag reduction. The final aim is to reduce the pressure drop required by an ESP.

In this paper, first, we review phenomena occurring in a boundary layer and one turbulence control strategy based on the use of large-scale structures. Second, we analyze the influence of large-scale electrohydrodynamically induced streamwise vortical flows superimposed on turbulent plane Poiseuille flow using direct numerical simulation. The EHD flows had a spanwise periodicity of 340 wall units, which is characteristic of ESP geometry. Regardless of intensity, EHD flows induce an initial transient of ~ 600 shear-based time units with moderate drag decrease ($\sim 6-7\%$), followed by a steady-state with slight drag modification. The behavior of the shear-stress at the wall was examined in connection with the shape of the EHD flows to identify future directions for further drag reduction.

INTRODUCTION

The study of the interaction between electrostatic body forces and turbulent flows has relevance in a number of applications, ranging from aerospace technology [1, 2] to electrostatic filtering [3, 4, 5, 6, 7].

Injecting ionic species into a gas and superimposing an electrostatic field leads to steady body force acting on the fluid. This phenomenon is common in electrostatic precipitators (ESP). In the most widely used configuration, an ESP is constituted by two vertical grounded plates through which the dust-laden gas flows horizontally. Regularly spaced, vertical thin wires are placed in the middle of the duct and are kept at high potential in order to discharge the ions required to charge the initially neutral airborne particles that are to be separated. Under common operating conditions, the ions discharged by the wires are accelerated towards the wall and generate spanwise plane jets which, in turn, produce spanwise two-dimensional vortices of the size of the wire-to-wall distance [3, 5, 6, 7]. In previous papers, we have shown that the application of increasing voltages to the wires led to a decrease in overall drag – the maximum reduction being about 6 % [6] – and to increasing mass transfer at the wall [8]. Drag reduction mechanisms were shown to be related to modifications in frequency and intensity of Reynolds-stress producing events.

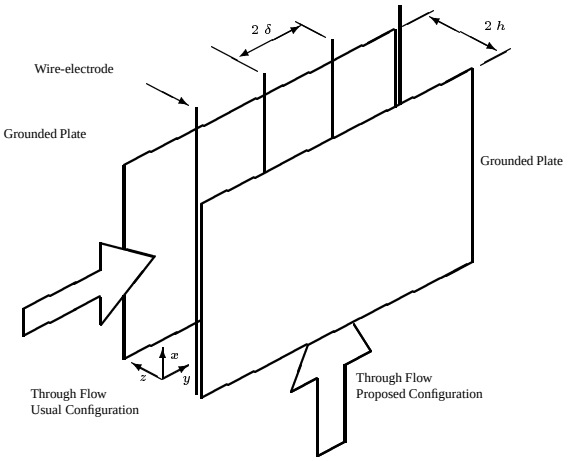

Figure 1: Schematics of wire-plate ESP with proposed new flow configuration.

In this paper, we examine the possibility of a new configuration for ESPs in which EHD flows produce vortical flows with a streamwise axis. In this configuration, shown in Figure 1, the main flow is directed parallel to the wires. This idea was prompted by the recent papers of Schoppa and Hussain [9, 10] who identified one of the possible cycles which controls low Reynolds number turbulence generation and proposed an idealized means for its control. In this cycle, low-speed streaks are subject to lateral instability and determine the generation of streamwise vortices which, in turn, sustain the streaky structures. Interrupting this cycle at a certain point would prevent the formation of the streamwise vortical structures and significantly decrease drag.

In this work, first, we present the mechanism of turbulence regeneration described by Schoppa and Hussain (1997) deriving the rationale for turbulence control and drag reduction. Second, we examine the possibility of reducing drag by electrostatic forces. We studied a pressure driven Poiseuille flow with streamwise axis vortical structures of EHD origin. This flow occurs in the new ESP configuration as shown in Figure 1. We analyzed this flow using a pseudospectral Direct Numerical Simulation (DNS). If the configuration shown in Figure 1 can be optimized for drag reduction, it could represent a significant improvement in ESP technology since pressure drop can be a significant parameter for the optimization of operative costs.

WALL TURBULENCE AND RATIONALE FOR CONTROL

In a turbulent boundary layer, momentum, heat and mass transfer are controlled by strong local motions of fluid which are called *ejections* and *sweeps*. These motions control turbulent mixing close to the wall: ejections bring the low-momentum fluid close to the wall into the outer region, whereas sweeps bring the high-momentum fluid from the outer flow into the wall region. Ejection-

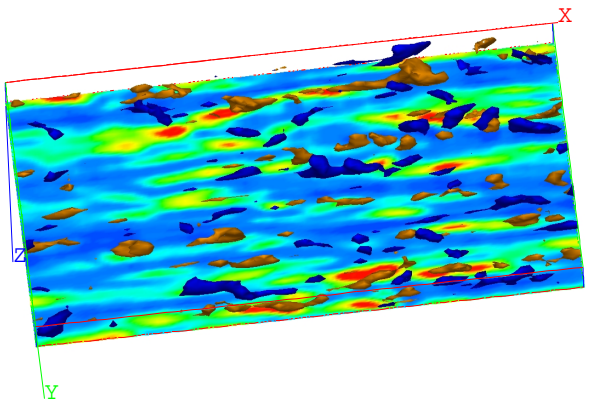

Figure 2: Instantaneous footprint of the wall shear-stress with corresponding sweep and ejection events in the whole computational domain. At the wall, red indicates high shear-stress; blue indicates low shear-stress. Gold 3D regions are isosurfaces characterizing sweeps whereas blue 3D regions characterize ejections. 3D isosurfaces are traced at $u'w' = -3$ in dimensionless units. A time-sequence animation of the events shown in this Figure may be retrieved at `http://www-cfd.dstc.uniud.it/www/movie1.htm`

Figure 3: Quasi-streamwise counterrotating vortices together with ejections and sweeps. Quasi-streamwise vortices extend for about $300\ x^+$. Two isosurfaces of the same absolute value of Ω indicate clockwise rotating (red) and counterclockwise rotating (pale blue) vortices. Sweeps and ejections are indicated by green and blue respectively. A time-sequence animation of the events shown in this Figure may be retrieved at `http://www-cfd.dstc.uniud.it/www/movie2.htm`

s and sweeps control momentum transfer at the wall and are also well correlated to heat transfer [11, 12] and mass transfer [13] at the wall. In Figure 2, the footprint of the shear-stress at the wall is shown together with sweep and ejection events. In this Figure, sweeps and ejections are identified with the same isocontour of the instantaneous surface at $u'w' = -3$. Low shear-stress regions correspond to the ejections – uplifting of low momentum fluid – whereas high shear-stress regions correspond to the sweeps – downwash of high momentum fluid. Both sweeps and ejections contribute to positive turbulence production.

There is still some uncertainty about the mechanisms which generate and maintain the sweep/ejection events. They appear to be generated by the quasi-streamwise vortices which populate the near wall region. Quasi-streamwise vortices have a characteristic length of about 200 wall units and a spacing of about 400 wall units [9, 14, 15]. These vortices are slightly tilted away from the wall and are responsible for pumping fluid towards and away from the wall. The streamwise vortices may be identified by calculating the eigenvalues of the strain rate tensor [16, 17, 18]. The vector Ω is related to the streamline rotation, represents the strength and direction of the rotation of the streamlines, and is associated with the complex eigenvalues of the strain rate tensor. In Figure 3, two counterrotating vortices, identified by one isosurface of Ω, are shown together with the ejections and sweeps they generate. The elongated red and pale blue structures are two isosurfaces with the same absolute value of Ω (and opposite sign) and indicate clockwise rotating (red) and counterclockwise rotating (pale blue) vortices. The blue lumps of fluid in between the two vortices are ejections and the green lumps of fluid outside the two vortices are sweeps.

Many quasi-streamwise vortices are usually associated with one single low-speed streak. Low-speed streaks are sinuous regions about 1000 wall units long and are characterized by a value of the streamwise velocity lower than the mean. Low-speed streaks alternate with high-speed regions, which are usually shorter. In Figure 4, quasi-streamwise vortices are shown associated with one low-speed streak – a 650 wall unit-long piece of one low-speed streak. Quasi-streamwise vortices are slightly tilted upward – about 9^o average [9]; clockwise and counterclockwise rotating vortices are also slightly tilted about 4^o right and left respectively. One single low-speed streak has a longer life than quasi-streamwise vortices and survives a number of vortex generations. In Figure 5, one single low-speed streak is shown for a length of about 1200 wall units. The isosurface indicates a streamwise velocity value of $0.56\ U_c$ where U_c is centerline velocity. The streak is sinuous and, in time, oscillates in the spanwise direction. The isosurface of the streak has different slope and shape at different locations. It has been shown [19] that the generation of the quasi-streamwise vortices is associated with changes in the shape of the low-speed streak surface. The Lagrangian evolution of the shape of a low-speed streak is shown in Figure 6. The section shown in Figure 6 a) is followed downstream with the velocity $0.56\ U_c$ [19]. During the sequence shown in Figure 6, the wall layer undergoes a quiescent phase, Figure 6 a) and b), during which there is no evidence of quasi-streamwise vortices, and an active phase, Figure 6 c), d) and e), during which there is an alternate appearance of quasi-streamwise vortices of opposite sign, and again a quiescent phase, Figure 6 f). It is interesting to observe that clockwise and counterclockwise rotating vortices do not appear at the same time at the same location, as discussed by Schoppa and Hussain [9]. During the whole cycle, the section of the streak was advected downstream for 640 wall units.

In a recent paper, Schoppa and Hussain (1997) suggested that wall turbulence is dominated by a cycle in which low-speed streaks generate quasi-streamwise vortices, which in turn generate ejections and sweeps. These finally contribute to maintain the low-speed streaks. A crucial question is how the low-speed streaks can gener-

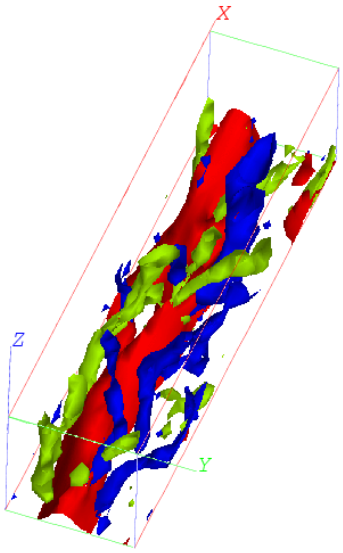

Figure 4: One low-speed streak (red) with counterrotating quasi-streamwise vortices in a box about Clockwise rotating vortices (blue) are on the right side of the low-speed streak and are slightly tilted right; Counterclockwise rotating vortices (green) are on the left side and are slightly tilted left.

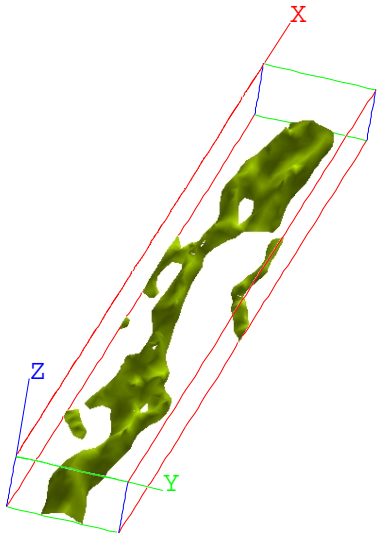

Figure 5: Velocity isosurface describing one isolated low-speed streak. Isosurface velocity value is $0.56\ U_c$. A time-sequence animation of the low-speed streak shown in this Figure may be retrieved at `http://www-cfd.dstc.uniud.it/www/movie4.htm`

ate the quasi-streamwise vortices. Schoppa and Hussain (1997) answer this by examining the behavior of a single low-speed streak and finding that it is subject to lateral, sinuous instability. Stability analysis of an idealized low-speed streak showed it to be unstable to lateral perturbations; basing their examination also on the DNS of a minimal channel-flow unit [20], the authors were able to demonstrate that a vortex-less streak is able to generate new streamwise vortices. They conclude by suggesting different strategies for turbulence control: the most interesting strategy seems to be stabilization of the low-speed streaks. This could be done in a number of ways but a large-scale approach seems more reasonable given the obvious technological advantages. The use of large-scale motions was already investigated by several authors, who exploited oscillating walls [21, 22, 23, 24]. In the DNS work by Jung et al. [21], drag was reduced up to 40%.

A different approach was suggested by Schoppa and Hussain [10] who, in a further paper, hypothesized that a large-scale, forcing velocity field in the spanwise direction would stabilize the streaks and block the turbulence regeneration cycle. To test this concept, they used synthetic streamwise vortical flows, with a spanwise wavelength of 400 wall units [10] and demonstrated that superimposing these induced flows on a turbulent boundary layer led to temporary but significant drag reduction. Starting from this background, we decided to investigate whereas electrostatic forces can be used to generate large-scale flows suitable to reduce turbulent drag.

In ESPs, the EHD flows are perceived as detrimental to operation. If EHD flows could be tuned in order to obtain the values and characteristics required to stabilize the low-speed streaks, their presence could turn into a benefit from the viewpoint of the pressure drop. Following our previous work [6], we used electrostatic forces to generate the large-scale structures imposed on the turbulent throughflow and we tried to simulate physical control flows with some of the characteristics suggested by Schoppa and Hussain (1998).

NUMERICAL SIMULATION

The turbulent flow of air, assumed to be incompressible, Newtonian, with no-slip conditions at walls, and driven by a pressure gradient, was numerically simulated for an imposed pressure gradient. The wire-electrodes necessary to generate the electrostatic body force to drive the control flows were kept at a potential sufficient to ensure ionic discharge and the presence of distributed ionic species in the duct. Ions are subjected to the Coulomb force, $\mathbf{F}$, which may be expressed as:

$$\mathbf{F} = \rho_c \mathbf{E} \quad , \tag{1}$$

where ρ_c is the charge density and $\mathbf{E}$ is the electric field vector. Ions are driven toward the walls and collide with fluid molecules, transferring momentum to them. This is equivalent to a body force which acts directly on the fluid. Therefore, the equation of fluid motion in dimensional terms is

$$\rho \left[\frac{\partial u_i}{\partial t} + u_j \frac{\partial u_i}{\partial x_j} \right] = -\frac{\partial \mathcal{P}}{\partial x_i} + \mu \frac{\partial^2 u_i}{\partial x_j \partial x_j} + F_i \quad , \tag{2}$$

where u_i are the dimensional velocity components along the three directions x_i (with x_1, or x being streamwise, x_2 or y being spanwise and x_3 or z being the wall-normal directions), $\mathcal{P}$ is pressure, and ρ and μ are fluid density and dynamic viscosity, respectively. For the case under consideration, the body force depends only on y and z, implying that the body force distribution does not fluctuate because of ionic convection. This is a realistic assumption, since ions have a drift velocity of about a hundred meters per second in air while the mean flow velocity is about one meter per second. For liquids, ionic convection may not be negligible in some situations and "two-way" coupling will exist between the flow field and the electrostatic body force field. Here the coupling is "one-way", *i.e.* the flow field does not modify the electrostatic body forces.

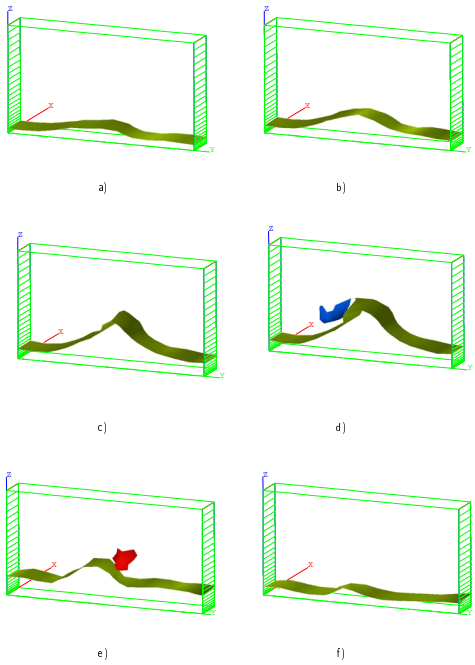

Figure 6: Lagrangian evolution of low-speed streak surface – identified by the $0.56\ U_c$ isosurface – associated with the presence of streamwise vortices – identified by the Ω isosurface, red is clockwise rotating and blue is counterclockwise rotating. The streamwise location is advected downstream with velocity $0.56\ U_c$ (Kim and Hussain, 1993). The wall units time of the different snapshots is a) time 0, b) time 24, c) time 52, d) time 94, e) time 131, and f) time 181. The wall region undergoes modifications from quiescent phase a) and b), to active phase, c), d) in which the presence of a counterclockwise rotating streamwise vortex is noted, and e) in which the presence of a clockwise rotating streamwise vortex is observed, back to quiescent phase, f). During the time sequence, the initial cross-section advanced about 640 wall units downstream.

FLOW FIELD

The flow field was calculated by integrating mass and momentum balance equations in dimensionless form obtained using the duct half-width, h, and the shear velocity, u_τ, defined as

$$u_\tau = \sqrt{\frac{\tau_w}{\rho}} \tag{3}$$

where τ_w is the shear at the wall. Therefore, mass and momentum balance equations in dimensionless form are

$$\frac{\partial u_i}{\partial x_i} = 0 \quad , \tag{4}$$

and

$$\frac{\partial u_i}{\partial t} = -u_j \frac{\partial u_i}{\partial x_j} + \frac{1}{Re} \frac{\partial^2 u_i}{\partial x_j \partial x_j} - \frac{\partial p}{\partial x_i} + \delta_{1,i} + \Phi_i \quad , \tag{5}$$

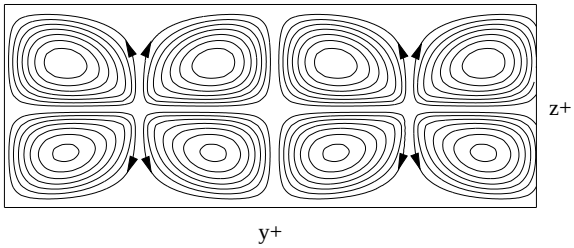

Figure 7: Streamlines of control flows for no-through flow C-3 case. Contours go from -35 to 35 with increments of 4 in wall units.

where u_i is the ith component of the dimensionless velocity vector, $\delta_{1,i}$ is the mean dimensionless pressure gradient, Φ is the dimensionless electrostatic body force, and $Re_\tau = hu_\tau/\nu$ is the shear Reynolds number. Eqs. 4 and 5 were solved directly using a pseudo-spectral method similar to that used by Kim *et al.* (1987) to solve the turbulent, closed-channel-flow problem. The difference is the inclusion of the space-dependent body force which, being steady and uncoupled to the flow field, was calculated once at the beginning of each simulation. If the body force term is treated together with the nonlinear terms, Eq. 5 may be recast as:

$$\frac{\partial u_i}{\partial t} = S_i + \frac{1}{Re_\tau} \frac{\partial^2 u_i}{\partial x_j \partial x_j} - \frac{\partial p}{\partial x_i} \tag{6}$$

which is identical to forms previously solved [25, 26], and where S_i now includes the convective term, the mean pressure gradient and the Coulomb term. The pseudo-spectral method is based on transforming the field variables into wave-number space, using Fourier representations for the streamwise and spanwise directions and a Chebyshev representation for the wall-normal (nonhomogeneous) direction. A two-level, explicit, Adams-Bashforth scheme for the nonlinear terms S_i and an implicit Crank-Nicolson method for the viscous terms were employed for time advancement. Details of the method have been published previously [26].

Considering air with density of $1.38\ kg/m^3$, and kinematic viscosity of $16.6 \cdot 10^{-6}\ m^2/s$, since the pressure gradient is imposed equal for all simulations, the shear velocity is $8.964 \cdot 10^{-2}\ m/s$, and the shear Reynolds number is equal to 108. For the reference case with no EHD effects, the mean velocity is $1.16\ m/s$ and the Reynolds number based on mean velocity and duct width is ~ 2795. The grid is $64 \times 64 \times 65$ in the streamwise, spanwise and wall normal directions, respectively.

BODY FORCE CONTROL FIELD

The electrostatic potential distribution and space charge distribution are given by the following set of equations:

$$\frac{\partial^2 V}{\partial x_i^2} = -\frac{\rho_c}{\epsilon_0} \tag{7}$$

	Current Dens. (A/m^2)	$W_{cont.}/W_{chan.}$ (%)
C1	1.00E-07	2.7
C2	5.00E-06	8.3
C3	2.00E-05	25.2
C4	5.00E-05	58.9

Table 1: Summary of the simulations

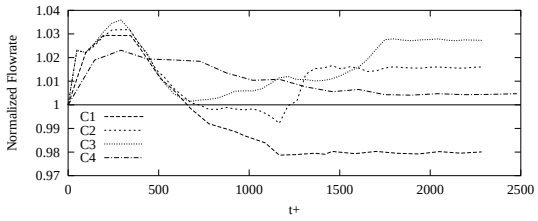

Figure 8: Time evolution of flowrate for the different cases. Flowrates are normalized by unforced channel flowrate. Initial increase is followed by a steady-state.

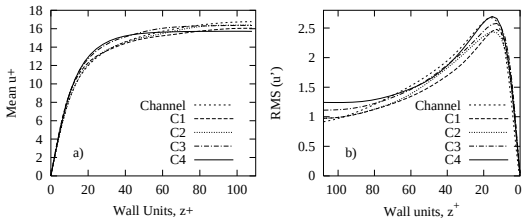

Figure 9: Statistics in actuated flow and unactuated flow. a) Mean velocity profiles; b) streamwise velocity fluctuations.

$$\rho_c^2 = \epsilon_0 \frac{\partial \rho_c}{\partial x_i}\frac{\partial V}{\partial x_i} \quad = - \quad \epsilon_0 \frac{\partial \rho_c}{\partial x_i} E_i \tag{8}$$

$$E_i = -\frac{\partial V}{\partial x_i} \tag{9}$$

$$J_i = -\rho_c \beta E_i \quad . \tag{10}$$

where, ϵ_0 is air permittivity ($\epsilon_0 = 8.854 \cdot 10^{-12}$), and $\beta = 1.4311 \cdot 10^{-4} m^2/V\ s$ is ionic mobility [28] for positive discharge in air. Eqs. 7-10 were solved by a two dimensional finite difference scheme [27] based on an initial guess for the space charge density at the wire followed by iterative solution of Eqs. 7 and 8 until convergence of the plate current density was obtained. Details on the numerical procedure and on the validation of the body force calculation against previous numerical and experimental analyses may be found in previous works [29]. The problem investigated is described by the balance equation for the fluid and a reduced set of Maxwell equations for the electrostatic body force distribution [6], which, being decoupled from the flow field, can be calculated once for all and regardless of how the flow field evolves. We use a two-dimensional finite-difference method to calculate the electrostatic body force field [6].

All simulations started from a channel-flow simulation, with no EHD flows calculated for a shear Reynolds number, $Re_\tau = 108$ over a grid of $64 \times 64 \times 65$ [30]. The body force is then applied and simulations run until a new steady state is reached. The wires are kept at a potential of $15\ 000\ V$ for all simulations – a potential typical in ESP applications – while the current flowing through the duct is varied. This allows control flows of different intensities. After the steady state is reached, simulations are continued for a sufficient number of time steps to obtain adequate statistics. In all simulations, the pressure gradient was maintained fixed, and corresponding to $Re_\tau = 108$.

The control variable in these simulations is the intensity of the electric current flowing through the duct. However, this information is not easy to relate to the structure of the turbulent flow field. The flowrate of the organized forcing flows is a better correlation parameter [10]. Since it is not straightforward to predict, *a priori*, the intensity and the distribution of the control flows once they have interacted with the turbulent throughflow, we characterized the control flows on the basis of the distribution and intensity for no throughflow. Current intensity and corresponding flowrates for the four cases investigated are reported in Table 1 for the no throughflow cases – current intensities are in the range normally used in ESPs. Flowrates are normalized by the flowrate of the channel with no imposed forcing flows. In Figure 7, the streamlines of the undisturbed forcing flows obtained for no throughflow and in laminar conditions are shown for case C3.

RESULTS

OVERALL DRAG MODIFICATION

Since the pressure drop is maintained the same for all simulations, all drag changes are indicated by the behavior of the flowrate: drag reduction is indicated by an increase of the flowrate, drag increase is indicated by a decrease of the flowrate. In Figure 8, the time-behavior of the flowrate normalized by the unforced case flowrate is shown for the different cases. After induction of EHD flows, there is a transient lasting about 600 dimensionless time units in which the mean velocity increases for all simulations. Some indications to explain such transient behavior may be found elsewhere [31]. At very low intensity, drag is increased, whereas for higher intensity drag is reduced. In cases C2 and C3 the mean velocity reaches a steady state with increases of 2% and 3% respectively. In case C4, the initial peak is lower and the slope toward the steady state is milder. A steady state is reached after about 15000 wall time units with practically no drag reduction compared to the unforced case. Thus, maximum drag reduction seems to exist for this type of forcing flows – conditions close to case C3.

MEAN VELOCITY AND TURBULENCE INTENSITY

The mean velocity for the unforced channel-flow case is compared against the mean velocity profiles of the forced cases in Figure 9 a). The profiles appear flattened in the center of the channel, but increase in the wall region, producing, in the three higher-potential cases, a net increase in the flowrate, as confirmed by Figure 8.

In the present simulations, energy is fed into the turbulence field by the mean pressure gradient and by the electrostatic forces. A careful examination of turbulence statistics, turbulence structure and energy and Reynolds stress budgets is advisable in order to establish the effects EHD flows have on the turbulence field and on the mean field. To do this analysis, a suitable method of filtering out the large-scale forcing flows should be adopted. The electrostatic field is two-dimensional and a filtering procedure could be averaging over the x direction. However, the streamwise EHD vortical flows have sizes comparable to those of the streamwise vortices typical of the boundary layer, with which they interact in a complex way. Averaging over the streamwise direction [6] allows identification of EHD flows only when they are much stronger than unforced case vortices – *i.e.* in case C4, which is not representative for all the other cases. Thus in Figure 9 b), we show only turbulence intensity in the streamwise direction, which is not directly modified by the EHD flows, since they have a null component in the x direction. In all cases, turbulence intensity decreases in the wall region and increases in the central region of the channel. Compared to the unforced channel-flow case, for increasing intensity of the control flows, there is an initial decrease

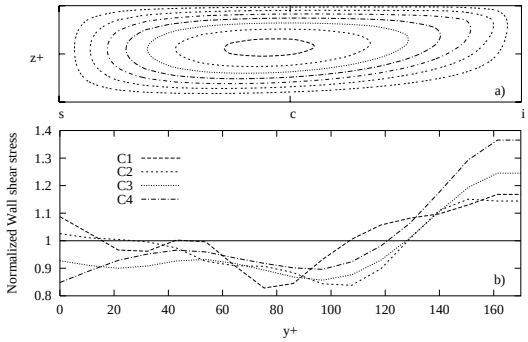

Figure 10: Influence of single EHD streamwise vortex on time-averaged wall shear-stress. a) undisturbed (no-through flow case) EHD vortex; b) time-average of wall shear-stress in each case normalized by time-average of wall shear-stress in unforced channel case.

of turbulence intensity in the wall region – cases C1 and C2 – followed by an increase in turbulence intensity in cases C3 and C4. This indicates that after initially damping turbulence production, higher intensity control flows increase turbulence levels, producing turbulence by their own mechanisms [6]. The peak in the unforced case is always larger than in the forced cases.

In their paper on the dynamics of wall coherent structures, Schoppa and Hussain [9] suggest that lateral forcing would be appropriate to reduce drag by damping the streak-regeneration mechanism. In their subsequent letter [10], they exploit large, mathematical vortices with streamwise axis and they analyze the influence these vortices have on turbulence in a specific way which we followed [32, 33] and present here to extrapolate an ideal forcing EHD flow. Consider Figure 10 a), where one single EHD-generated vortex is shown: the EHD jet impinges on the wall at "i", then the streamlines run parallel to the wall through "c" and they return toward the outer flow at "s". In Figure 10 b), the behavior of the normalized, time-averaged wall shear-stress is shown for each simulation. In all forced cases, the time-averaged wall shear-stress increases in the impingement region and decreases where the EHD flow streamlines are parallel to the wall. In the lower intensity cases, C1 and C2, the wall shear-stress increases again close to point "s". Following the definition of Schoppa and Hussain [10], we can name the "i-s" region in Figure 10 a) as vortex forcing and the "c-s" region in Figure 10 a) as wall-jet forcing. In case C4, the time-averaged wall shear-stress in the "c-s" region is about 0.90% of that in the unforced case. In case C3, which is the most favorable, the time-averaged wall shear-stress in the "c-s" region is about 0.87% of that in the unforced case. Apparently, the wall shear-stress is significantly reduced in the region where the forcing flow is parallel to the wall – as suggested by Schoppa and Hussain [9] – but it is greatly increased in the region where extra drag is generated by the EHD jet impinging on the wall. This increase is, in most cases, sufficient to reduce the beneficial effect to a few percent drag reduction.

CONCLUSIONS

In this work, we tried to exploit using a physical mechanism the idealized strategy for turbulence control presented by Schoppa and Hussain [10]. This strategy is based on the use of large-scale, wall parallel jets to stabilize the low-speed streaks which have been shown responsible for one of the mechanisms generating and maintaining turbulence. The wall-parallel jet could be part of a large-scale vortex with streamwise axis. This type of vortex can be generated in electrostatic precipitators, where dispersed ions are subject to the action of the applied electrostatic field. Usually, ESPs exhibit large-scale vortices with spanwise axis: in this work, we propose a new configuration for ESPs in which the vortices have streamwise axis. This configuration can be optimized for drag reduction and could represent a significant improvement in ESP technology.

We have performed DNS of the turbulent Poiseuille flow coupled to the Maxwell equations required to calculate the body forces which maintain the EHD flows, and we have shown that EHD-induced, streamwise vortical flows may be used to modify turbulence characteristics, even though in the specific configuration examined, which is of interest for ESP design, did not lead to dramatic changes in drag.

At present, we are looking at various geometrical configurations which could increase the extent of wall-parallel jets and reduce the extra drag generated by the EHD jets impinging on the wall, focusing on finding an optimized configuration for drag reduction. This includes using wall-parallel jets and oscillating the electrostatic field with suitable frequencies.

ACKNOWLEDGMENT

The author would like to thank Cristian Marchioli and Marco Fulgosi, now at ETH, Zurich, for performing calculations and visualizations. Computational resources provided by ENEL/CRT, Pisa, Italy on their CRAY T94/164 are gratefully acknowledged.

Bibliography

[1] Malik, M. R., Weinstein, L. M., and Hussaini, M. Y. (1983). Ion wind drag reduction. *AIAA 83-0231* , 21^{th} Aerospace Sciences Meeting, January 10-13, 1983, Reno (NV) (1983)

[2] Roth, J. R., Sherman, D. M., and Wilkinson, S. P. (1998). Boundary layer flow control with a one atmosphere uniform glow discharge surface plasma. *AIAA 98-0328* , 36^{th} Aerospace Sciences Meeting, January 12-15, 1998, Reno (NV) (1998)

[3] Yamamoto, T. and Velkoff, H. R. (1981). Electrohydrodynamics in an electrostatic precipitator. *J. Fluid Mech.* , **9**, 108–122.

[4] Leonard, G. L., Mitchner, M., and Self, S. A. (1983). An experimental study of the electrohydrodynamic flow in electrostatic precipitators. *J. Fluid Mech.*, **127**, 123–145.

[5] Kallio, G. A. and Stock, D. E. (1992). Interaction of electrostatic and fluid dynamic fields in wire-plate electrostatic precipitators *J. Fluid Mech.* , **240**, 133–153.

[6] Soldati, A. and Banerjee, S. (1998). Turbulence modification by large scale organized electrohydrodynamic flows. *Phys. Fluids* , **10**, 1742–1756.

[7] Soldati, A. (2000). On the effects of electrohydrodynamic flows and turbulence on aerosol transport and collection in wire-plate electrostatic precipitators *J. Aerosol Sci.* , **31**, 293–305.

[8] Soldati, A. (1998). Turbulence control and drag reduction by means of large-scale EHD Structures *International Workshop on Electrical Conduction, Convection and Breakdown in Fluids*, Seville (Spain), Mar. 27-28, 1998, pp. 119.

[9] Schoppa, W. and Hussain, F. (1997). Genesis and dynamics of coherent structures in near-wall turbulence. In *Self-sustaining Mechanisms of Wall Turbulence* , Ed. R. Panton, Computational Mechanics Publications, p. 385–422.

[10] Schoppa, W. and Hussain, F. (1998). A large-scale control strategy for drag reduction in turbulent boundary layers. *Phys. Fluids* , **10**, 1049–1051.

[11] Papavassiliou, D. V. and Hanratty, T. J. (1995). The use of Lagrangian methods to describe turbulent transport of heat from a wall. *Ind. Eng. Chem. Res.*, **34**, 3359–3367.

[12] Kasagi, N. and Iida, O. (1999). Progress in Direct Numerical Simulation of Turbulent Heat Transfer. Keynote Paper, 5^{th} ASME/JSME Joint Thermal Engineering Conference, San Diego, CD-ROM Publication, ASME, March, 1999.

[13] De Angelis, V., Lombardi, P., Andreussi, P. and Banerjee, S. (1997). Mycrophysics of scalar transfer at air-water interfaces. Invited Paper, IMA Conference on *Wind over Wave Couplings* , Salford, UK, 8-10 April, 1997, Oxford University Press (In Press).

[14] Jeong, J., Hussain, F., Schoppa, W., and Kim, J. (1997). Coherent structures near the wall in a turbulent channel flow. *J. Fluid Mech.* , **322**, 185–202.

[15] Jimenez, J. and Pinelli, A. (1999). The autonomous cycle of near-wall turbulence *J. Fluid Mech.* , **389**, 335–359.

[16] Perry, A. and Chong, M. S. (1987). A description of eddying motions and flow patterns using critical point concepts. *Annu. Rev. Fluid Mech.* , **9**, 125–148.

[17] Chong, M. S., Perry, A., and Cantwell, B. J. (1990). A general classifiction of three-dimensional flow fields *Phys. Fluids A*, **2**, 765–777.

[18] Jeong, J. and Hussain, F. (1995). On the identification of a vortex. *J. Fluid Mech.* , **285**, 69–83.

[19] Kim, J. and Hussain, F. (1987). Propagation velocity of perturbations in turbulent channel flow. *Phys. Fluids A*, **5**, 695–706.

[20] Jimenez, J. and Moin, P. (1991). The minimal flow unit in near-wall turbulence *J. Fluid Mech.* , **225**, 213–233.

[21] Jung, W., Mangiavacchi, N., and Akhavan, R. (1992). Suppression of turbulence in wall-bounded flows by high frequency spanwise oscillations *Phys. Fluids A*, **4**, 1605–1607.

[22] Baron, A. and Quadrio, M. (1995). Turbulent drag reduction by spanwise wall oscillations. *Appl. Sci. Res.*, **4**, 311–326.

[23] Choi, K-S. and Graham, M. (1998). Drag reduction of turbulent pipe flows by circular-wall oscillation. *Phys. Fluids* , **10**, 7–9.

[24] Mito, Y. and Kasagi, N. (1998). DNS study of turbulence modification with streamwise-uniform sinusoidal wall-oscillation. *Int. J. Heat Fluid Flow* , **9**, 470–483.

[25] Kim, J., Moin, P., and Moser, R. (1987). Turbulence statistics in fully developed channel flow at low Reynolds number. *J. Fluid Mech.* , **177**, 133–166.

[26] Lam, K. and Banerjee, S. (1992). On the condition of streak formation in bounded flows. *Phys. Fluids A*, **4**, 306–320.

[27] Leutert, G. and Bohlen, B. (1972). The spatial trend of electric field strength and space charge density in plate type electrostatic precipitator. *Staub Reinhalt Luft*, **32**, 27–34 (In English).

[28] Mc Daniel, E. W. and Mason, E. A. (1973). *The mobility and diffusion of ions in gases* New York, NY, Wiley.

[29] Kallio, G. A. and Stock, D. E. (1986). Computation of electrical conditions inside wire-duct electrostatic precipitators using a combined finite-element, finite-difference technique *J. Appl. Phys.* , **59**, 1799–1806.

[30] Soldati, A. Andreussi, P. and Banerjee, S. (1993). Direct simulation of turbulent particle transport in electrostatic precipitators. *AIChE J.* , 1910–1919.

[31] Coleman, G.N., Kim, J., and Le, A.T. (1996). A numerical study of three-dimensional bounded flows. *Int. J. Heat and Fluid Flow*, **17**, 333–342.

[32] Fulgosi, M., Banerjee, S., and Soldati, A. (1999). Turbulence modulation by an array of large-scale streamwise structures of EHD origin. *ASME Paper No. FEDSM99-6934* , 3^{rd} ASME/JSME Fluids Engineering Conference, San Francisco, CA, July, 18-22, 1999.

[33] Soldati, A. and Banerjee, S. (1999). Modulation of turbulent plane Poiseuille flow by large-scale streamwise electrohydrodynamic vortical flows. (Submitted).